Onset of magnetism in B2 transition metals aluminides

N. I. Kulikov,
Institute of High Pressure Physics, Troitsk, Moscow region, 142092, Russia

A. V. Postnikov, G. Borstel, and J. Braun
Fachbereich Physik, Universität Osnabrück, D-49069 Osnabrück, Germany
(Received December 23, 1997; in final form October 14, 1998)

Ab initio calculation results for the electronic structure of disordered bcc Fe_xAl_{1-x} ($0.4 < x < 0.75$), Co_xAl_{1-x} and Ni_xAl_{1-x} (x=0.4; 0.5; 0.6) alloys near the 1:1 stoichiometry, as well as of the ordered B2 (FeAl, CoAl, NiAl) phases with point defects are presented. The calculations were performed using the coherent potential approximation within the Korringa-Kohn-Rostoker method (KKR-CPA) for the disordered case and the tight-binding linear muffin-tin orbital (TB-LMTO) method for the intermetallic compounds. We studied in particular the onset of magnetism in Fe–Al and Co–Al systems as a function of the defect structure. We found the appearance of large local magnetic moments associated with the transition metal (TM) antisite defect in FeAl and CoAl compounds, in agreement with the experimental findings. Moreover, we found that any vacancies on both sublattices enhance the magnetic moments via reducing the charge transfer to a TM atom. Disordered Fe–Al alloys are ferromagnetically ordered for the whole range of composition studied, whereas Co–Al becomes magnetic only for Co concentration ≥ 0.5.

75.20.En 75.50.Bb 71.23.-k 71.15.Mb

I. INTRODUCTION

The intermetallic compounds FeAl, CoAl and NiAl attract considerable attention due to their uncommon properties. For example, a high melting point makes them attractive as promising high-temperature aerospace materials. Furthermore, an unusual magnetic behavior, depending on temperature and concentration, has been observed. The β-phase of these aluminides crystallizes in the B2 (CsCl) structure and persists over 45–58 at.% in the case of Co; β-phases of Ni and Fe aluminides are stable over a broader range of composition. It is known that these compounds have high concentrations of point defects, and moreover exhibit specific defect structures known as triple defects.[1] Predominant are apparently combinations of so-called antistructure (AS) atoms – usually transition metal (TM) atoms substituting Al (in the Al-poor region of the β phase), and vacancies on transition-metal sites (in the Al-rich region).

In spite of their structural similarity, these materials exhibit different mechanical and magnetic properties. At low temperatures (below 10 K), the nearly equiatomic alloy $Co_{0.506}Al_{0.494}$ shows a temperature dependence of the magnetic susceptibility which coincides neither with the Curie nor with the Curie-Weiss law.[2] There is a common agreement in the literature that the perfectly ordered compound CoAl is nonmagnetic,[3,4] but already a small disorder leads to the onset of local moments (see, e.g., Ref. 5 and references therein). Also it is widely believed that the Co-AS atoms are responsible for the magnetic properties of this compound: several authors tried to deduce from magnetic measurements the moment per Co-AS atom which is associated with an effective moment of $5\mu_B$.[2,3] It is necessary to note that above 60 at.% Co, a permanent magnetization appears at low temperatures.[3] For the NiAl case, no magnetic moment has been observed for any concentrations. Earlier *ab initio* calculations for ordered FeAl[6,7] reveal a moderate magnetic moment of 0.6–0.7 μ_B at the Fe site and a ferromagnetic ordering. Ordered CoAl and NiAl were found in earlier *ab initio* calculations to be nonmagnetic, which is in agreement with the measurements.

The experimental magnetic phase diagram shows that FeAl near stoichiometry is in a spin-glass phase,[8] but in cold-worked disordered Fe-Al alloys the saturation magnetization persists in both stoichiometric FeAl and Al-rich alloys.[9]

The concentration dependence of the lattice parameter for the β-phase of aluminides is also not trivial. Typically, one should expect some slight deviations from the Vegard's rule, i.e. nearly linear variation with composition. In CoAl and NiAl however, the lattice spacing has the maximum at approximately equiatomic concentration of the alloy.[10,11] In FeAl, the lattice constant is nearly constant over a wide range of composition from 30 to 51 at.% Al.[9] This fact has so far no theoretical explanation. Nevertheless one may expect such behavior to be due to the lattice dilatation, depending on the concentration of vacancies and antisite (AS) atoms, that in its turn is controlled by composition and heat treatment.

The microscopic understanding of these phenomena can be obtained from electronic structure calculations. Actually the electronic structure of magnetic TM aluminides with stoichiometric composition has been already studied for many times by various methods in different approximations. In the earliest calculations within the Korringa-Kohn-Rostoker (KKR)[12] and modified KKR methods[13] the problem of filling up of the TM d-bands by Al p-electrons was discussed in detail and the charge transfer was shown from an Al to a TM

site. The possibility of magnetic ordering was studied for the Ni–Al system by the augmented spherical wave (ASW) method[14]. Hereby only for Ni_3Al a ferromagnetic ordering was found, with a value of the Ni magnetic moment by an order of magnitude less than in pure Ni. Optical properties of TM aluminides were studied by the linear muffin-tin orbital (LMTO) method[15] and by the linearized-augmented-plane-wave (LAPW) method[16] for NiAl and CoAl. The experimental absorption maxima were found to be correlated to the band structure of these alloys.[17] Further details of the electronic structure of these compounds were studied by comparing the data from electron energy-loss spectroscopy with theoretical investigations performed by the LMTO method.[18] The trends in the chemical bonding and the phase stability of transition metal aluminides with equiatomic composition have been studied by the full-potential linearized augmented plane-wave (FLAPW) method.[7] A review of electronic structure calculation results, along with band structures, densities of states and Fermi surfaces of many TM aluminides can be found in Ref.[19]. A recent study using the full-potential linearized augmented Slater-type orbital method[20] reports the formation energies and equilibrium volume of many $3d$ aluminides.

The equation of state and all zero-pressure elastic moduli for CoAl have been calculated[21] also using the FLAPW method. In addition, cohesive, electronic and magnetic properties of the transition metal aluminides have been calculated using the tight-binding linear muffin-tin orbital (TB-LMTO) method.[6] Here it was found that only FeAl retains a magnetic moment, which has been mentioned above. These findings coincide with the results of earlier LMTO calculations for NiAl and FeAl intermetallic compounds[22] and with *ab initio* pseudopotential calculations[23] for CoAl.

There are relatively few calculations aimed at the study of defects' influence on the electronic and magnetic structure of TM aluminides. *Ab initio* electronic structure calculations for point defects in CoAl have been performed by Stefanou *et al.*[5] within the KKR-Green's function method. Herein the perturbation of the potential was included at the sites which are nearest to the substitutional impurity. Earlier, Koenig *et al.*[24] performed Green's function calculations for vacancies in B2 aluminides by the LMTO-Green's function method, but allowing only the potential at the impurity site to be perturbed. The LMTO method has been applied to study the electronic structure of AS defects in FeAl where the point defect was modelled by suitably chosen supercells.[25] Finally, the LMTO-CPA technique has been used for the calculation of electronic and thermodynamic properties of disordered NiAl alloys.[26] In Ref. 27, the LMTO-CPA calculation results are presented for discussing the order-disorder transition in FeAl alloys.

The supercell approach has been used in order to study the antiphase boundary in NiAl and FeAl[28,29] as well as point defects in these aluminides.[29] Very interesting results for the magnetism of Co-doped NiAl by FLAPW supercell calculation have been obtained by Singh,[30] and we compare our findings with these results.

Although many studies have been performed up to now, the aspects of magnetism seen as a function of concentration remains not completely clear in these compounds. The purpose of this paper is therefore to investigate the onset of magnetism in the β-phase of ferromagnetic TM (Fe, Co, Ni) aluminides. First-principles total energy calculations have been performed in order to determine the magnetic phase stability of these alloys. The calculations are based on the density-functional (DF) theory. We have applied the TB-LMTO method in order to solve the DF equations in the case of near-stoichiometric ordered compounds with points defects. The KKR-CPA has been used for disordered substitutional alloys. We also present here the results of our supercell simulations for AS atoms and vacancies for both sublattices of the ordered compounds and compare them with the results for completely disordered alloys in order to clarify the physical reasons for the magnetic instability in these systems.

This paper is organized as follows: Sec. II is devoted to the description of our calculational methods, in Sec. III we discuss the results of our TB-LMTO calculations for the point defects. In Sec. IV we present the results for disordered alloys, concentrating on Co-Al as the most interesting one. A summary is given in Sec. V.

II. METHODS OF CALCULATION

The conventional *linear muffin-tin orbital* method in the *atomic spheres approximation* (LMTO-ASA) as well as its tight-binding formulation (TB-LMTO) have been well described in the literature.[31,32] Here we present only the relevant computational details.

We have used equal and space-filling atomic sphere radii on Al and TM sites in all calculations, scaling them with the lattice constant when studying the volume trends. According to the experience of previous studies (see, e.g. Ref. 33), this choice gives the best description of electronic densities for these systems in the ASA. Basis functions up to $l = 2$ were included for both constituent atoms explicitly, and the $l = 3$ functions via the down-folding procedure.[34] Combined corrections have been included throughout, and the effect of non-local corrections (after Langreth and Mehl, Ref. 35) to the local density approximation (LDA), i.e. compared with the exchange-correlation potential by von Barth and Hedin,[36] has been specially addressed and discussed. Since the advent of schemes incorporating the non-local functional forms of the exchange-correlation energy in terms of electron density, they have been applied to many solid-state problems, including magnetic ones. Whereas the non-local corrections were shown to improve the LDA-based description in many cases (providing, e.g., the correct total energy hierarchies of magnetic phases), one should

keep in mind that they tend to underestimate the bonding and hence to lead to an overestimated equilibrium volume (otherwise typically underestimated within the LDA). Moreover, the non-local corrections favor larger magnetic polarization. In some systems, where the interplay of magnetic properties and volume is crucial, one must be careful in applying the non-local-corrected schemes. In the present study, we in many cases refer to the results obtained both within the LDA and incorporating the non-local corrections. Taken together, they provide reasonable error bars for the properties obtainable from a first-principle calculation scheme.

The tetrahedron method integration[37] have been performed on the $16\times16\times16$ mesh over the Brillouin zone (BZ), so that the total energy values cited below were converged against the k-mesh enhancement within relevant digits, important for the study of the volume trends.

The electronic structure of disordered Co–Al alloys have been calculated using the fast KKR-CPA technique.[38] The KKR-CPA method is based on the multiple scattering theory. In this case the electronic Green's function has to be calculated self-consistently with the scattering path operator for an atom embedded into the ordered lattice of effective scatterers. In addition, the potential for each constituent has to be brought to self-consistency in the CPA sense. Therefore in KKR-CPA we have two self-consistent procedures, that leads to a number of numerical difficulties. An effective solution of this problem has been proposed in Ref. 38. Specifically, for the BZ integration the tetrahedron scheme with complex energies is applied, and in the CPA loop the extrapolation approach with only few iterations is introduced in order to solve the CPA equation on the rectangular contour in the complex energy plane. As a rule, we used in the present work the same parameters for the energy integration contour as described in Ref. 38. The necessarily minimal basis set included s, p, d and f orbitals for both TM and Al atoms, at which all space-filling atomic spheres had the same size. In this sense, the calculation setup was close to that used in TB-LMTO calculations for the ordered structures. Another similarity is that no frozen core approximation has been used, i.e. both schemes are all-electron ones. The difference is, TB-LMTO calculations were scalar-relativistic ones whereas KKR-CPA calculations were nonrelativistic, but this difference seems to have only negligible effect on structural and magnetic properties of TM aluminides. Also, the effects of non-local density functionals have not been studied in our KKR-CPA calculations. The exchange-correlation has been treated there in the LDA according to the Hedin–Lundqvist prescription[39] for non-magnetic systems and with spin scaling after von Barth and Hedin[36] for magnetic alloys.

In contrast to the LMTO method where all energy eigenvalues are explicitly provided by matrix diagonalization and the application of the tetrahedron method is straightforward, the BZ integration is more involved in the KKR method. In order to trace the *a priori* unknown number of poles in the energy-dependent determinant, we have divided the irreducible part of the BZ into 1024 equivalent tetrahedra by an uniformly distributed mesh of k-points. While examining the tetrahedra one by one, we have divided those where the phase of the integrand changes by more than $\pi/3$ over the volume into eight smaller tetrahedra, etc. This subdivision allows us to reduce the number of k-points necessary to obtain the relevant precision by a factor of 2–2.5.

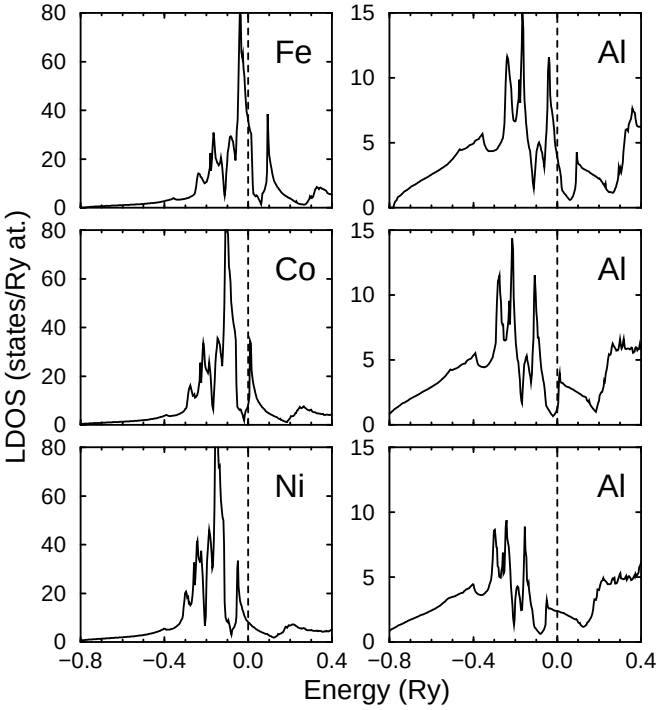

FIG. 1. Local DOS of components in the non-magnetic case for ordered FeAl, CoAl and NiAl as calculated by TB-LMTO. The dashed line indicates the Fermi level.

In consequence, 10–20 iterations using the modified Broyden scheme[40] for accelerating the convergence have been sufficient in the potential loop, at which the CPA self-consistency being achieved inside each iteration for the potential. The charge self-consistency has been used as the convergency criterion, and the iterations have been performed until the electronic density differences were stable to within 10^{-7}. Apart from conventional total energy and electronic structure calculations within the CPA, we have used the fixed-spin-moment (FSM) procedure[41] in order to analyze the volume/magnetic moment total energy dependence in Co–Al alloys.

III. ELECTRONIC STRUCTURE OF POINT DEFECTS IN CoAl AND FeAl COMPOUNDS

The above cited previous calculations of ordered FeAl, CoAl and NiAl compounds have shown that their electronic structures are rather similar and related roughly

by a rigid-band shift, which is depending on the number of conduction electrons and hence on the placement of the Fermi energy. This is illustrated by the electronic densities of states (DOS) for these materials, which are shown in Fig. 1. The ferromagnetism of FeAl is perfectly consistent with the Stoner model, as the Fermi level crosses the highest peak of a pronouncedly two-peak DOS distribution. For CoAl and NiAl, the Fermi level is outside of the region which is favorable for the onset of ferromagnetism.

Singh[30] emphasized the existence of a peak in the "rigid" DOS between the positions of the Fermi level in CoAl and NiAl. One can expect that tuning the number of conduction electrons, e.g. doping NiAl with Co, would favor the appearance of the magnetic order. In Ref. 30, for example, the effect of substitutional Co in NiAl has been investigated in a sequence of supercell calculations with the FLAPW method. An instability against ferromagnetism was found for $Co_{0.25}Ni_{0.75}Al$ and $Co_{0.125}Ni_{0.875}Al$ compositions. Apart from this, strong deviations from the rigid-band behavior were found for doped systems, implicating that the onset of magnetism in these systems may also be strongly dependent on the short-range order.

In the present study, we are primarily interested in the influence of local defects (vacancies and antisites),

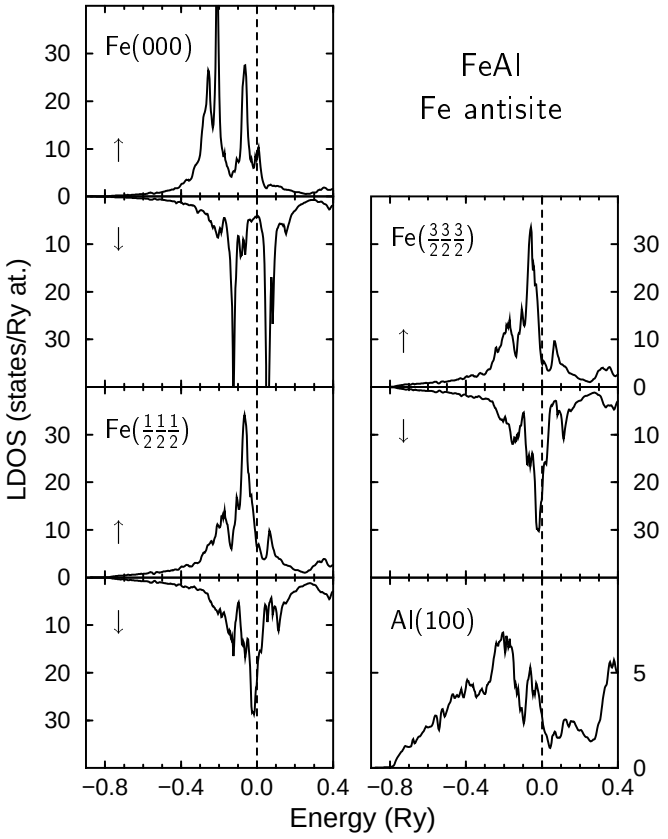

FIG. 2. Local DOS at the AS Fe defect and its several neighbors in FeAl as calculated by TB-LMTO. The dashed line indicates the Fermi level.

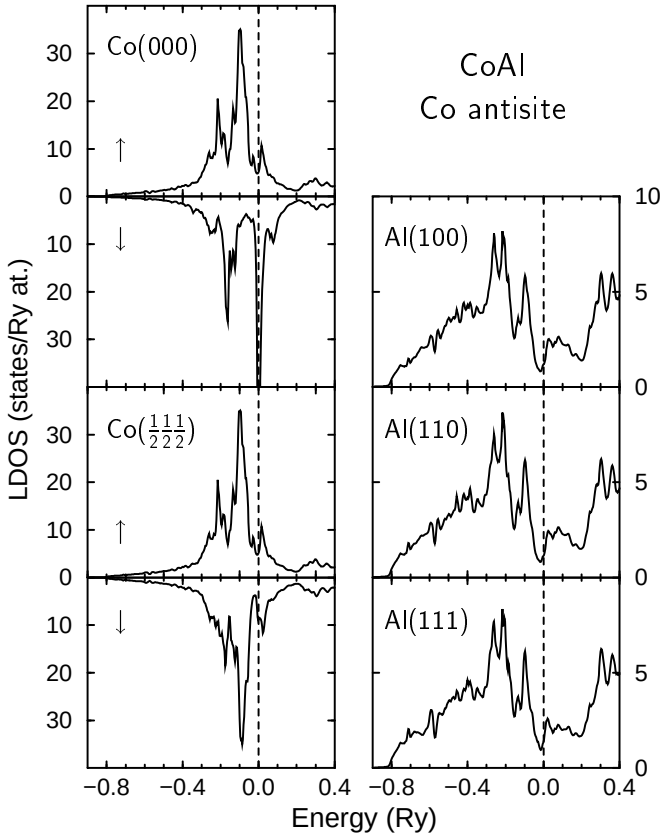

FIG. 3. Local DOS at the AS Co defect and its several neighbors in CoAl as calculated by TB-LMTO. The dashed line indicates the Fermi level.

which we have introduced on both sublattices in FeAl as well as in CoAl. In order to suppress the defect-defect interactions, quite large supercells have been used. For examining the energetics (i.e., optimizing the lattice spacing for different defect configurations), we have used supercells with translation vectors $(0, 2a, 2a)$, $(2a, 0, 2a)$, $(2a, 2a, 0)$ of the underlying cubic lattice, i.e. including 32 atoms. For reasons of controlling and for the thorough study of the spatial charge and magnetic moment distribution, we have performed several calculations with twice larger supercells, spanned up by the translation vectors $(-2a, 2a, 2a)$, $(2a, -2a, 2a)$, $(2a, 2a, -2a)$. In the last case, the next translated defect appears only as the 9th nearest neighbor within the corresponding sublattice. Since the calculations are fully self-consistent, they do probably provide a more accurate description of the screening of defects as was previously obtained with the use of KKR–Green's function method,[5] where the potentials only at the defect site and its nearest neighbors were allowed to deviate from the perfect-crystal values.

It should be noted that in the present treatment we did not account for a possible lattice relaxation of neighboring atoms around a vacancy of any type, keeping in mind that such relaxation cannot be reliably addressed in the ASA. To our knowledge, no such relaxation studies (with

TABLE I. Uncompensated number of electrons in the atomic sphere Q and local magnetic moments m in perfect ordered FeAl, CoAl and over shells of atoms around point defects in these alloys. The results are from 32-atom supercell calculations with nonlocal exchange-correlation potential and a=5.40 a.u.

Distance, units of a	Atom	FeAl				CoAl		
		Q	m, μ_B	Q	m, μ_B	Q	m, μ_B	Q
Sites in perfect bulk:		Fe		Al		Co		Al
		−0.240	0.761	0.240	−0.036	−0.330	0	0.330
		Fe-antisite		Al-vacancy		Co-antisite		Al-vacancy
0.000	TM or Vac.	−0.021	2.239	−1.089	0.029	−0.061	1.526	−1.047
0.866	TM	−0.204	0.759	−0.019	1.406	−0.280	0.143	−0.131
1.658		−0.247	0.648	−0.284	0.534	−0.337	0.027	−0.358
1.000	Al	0.254	−0.039	0.288	−0.052	0.350	−0.011	0.387
1.414		0.235	−0.042	0.200	−0.051	0.325	−0.010	0.296
1.732		0.233	−0.028	0.178	−0.049	0.316	−0.001	0.269
2.000		0.236	−0.023	0.236	−0.038	0.324	−0.004	0.319
		Al-antisite		Fe-vacancy		Al-antisite		Co-vacancy
0.000	Al or Vac.	0.180	−0.022	−1.064	−0.006	0.157	0	−1.076
0.866	Al	0.204	−0.027	0.382	−0.026	0.278	0	0.454
1.658		0.250	−0.034	0.215	−0.046	0.343	0	0.313
1.000	TM	−0.282	0.392	−0.204	0.838	−0.373	0	−0.310
1.414		−0.242	0.643	−0.282	0.635	−0.322	0	−0.350
1.732		−0.234	0.758	−0.299	0.603	−0.316	0	−0.370
2.000		−0.202	1.199	−0.206	1.454	−0.333	0	−0.358

the use of any full-potential scheme) have yet been done for the systems in question. According to Ref. 29, the relaxation around Pd vacancies in PdAl is up to 2.5%, and expectedly even less in FeAl, i.e. too small to have a noticeable effect on magnetic moments.

As most interesting examples related to the development of magnetic properties, the local DOS at different spheres around Fe and Co AS impurities in FeAl and CoAl are shown in Fig. 2 and 3, correspondingly. The numerical data for charge transfer values and magnetic moments inside atomic spheres of all defect systems studied are presented in Table I. These data correspond to the lattice constant a=5.40 a.u. that is about the equilibrium value for both ordered FeAl and CoAl. In the discussion that concerns the bulk properties and defect formation energies (see below) we refer to optimized equilibrium lattice spacings for defect systems, but this is not so important for discussing partial charges. The asymptotic value of the charge transfer within the perfect bulk is roughly recovered in the crystal away from defects. Some fluctuations in both charge transfer and magnetic moments however prevail and are discussed below.

It is well known that the charge transfer is not uniquely determined, since it depends on the choice of atomic spheres or cells between which the charge flow occurs. Moreover, because of different localization degree and spatial distribution of charge in different solids it doesn't make sense to discuss the charge transfer accompanying, e.g., the formation of a compound from elemental constituents. This has been discussed at length by Schulz and Davenport for 3d aluminides in Ref. 42. With this in mind, we compare in Table I the uncompensated charges Q in equal-sized atomic spheres at Al and TM sites in perfectly ordered aluminides. Charge-induced perturbations (Friedel oscillations) around the defects also can be found in Table I. We emphasize that not the absolute values of Q, but their changes over shells of neighbors to a defect are meaningful and of primary interest here. The interesting feature seen in Table I is that both Fe-AS and Al-AS defects are less charged as compared to respective bulk atoms of the ordered alloy. This is not surprising because the electro-negativity of the nearest neighbors is the same in both cases.

The general trends for the Fe–Al system could be already expected based on the rigid-band model. Since the electron transfer in the ordered alloy occurs from Al to TM, the ways to lower the concentration of electrons at the TM site are substitution of Al with a TM atom, or vacancies of any kind. The Al-AS substitution, on the other hand, is unfavorable for magnetism, as can be seen from Table I. The Fermi energy in ordered FeAl crosses the upper slope of a high peak. According to the rigid band picture, the decrease in the Al→Fe charge transfer leads to an increase of the local DOS value at the Fermi energy and thus favor the increase in the magnetic moment in the framework of Stoner theory.

Consistently with this it is seen from Table I that the magnetic moment of Fe as an AS defect (see also Fig. 2) or as a neighbor to the Al vacancy is enhanced simultaneously with the decrease of the charge transfer onto these sites. Because of such a locally changed charge transfer the *local* DOS at the defect site is affected in a rather complicated way, different from what one would expect from rigid-band considerations. The local DOS at the AS Fe, which is the central atom of the Fe_9 nearest-neighbor cluster, acquires certain similarity with the DOS of pure

bcc Fe with its half-filled minority-spin subband. Furthermore the magnitude of the local magnetic moment is quite close to that of bulk Fe. This is consistent with the fact that practically no charge transfer occurs between the central Fe atom and its nearest neighbors. From the experimental studies[43] the local moment has been estimated to fall within the range of 4 to 5.4 $\mu_{\rm B}$, depending on the vacancy concentration. According to our calculation, the cluster of nine Fe atoms including the AS develops 8.3 $\mu_{\rm B}$. The local DOS of Fe atoms which are more distant from the defect [Fe($\frac{1}{2}\frac{1}{2}\frac{1}{2}$) and Fe($\frac{3}{2}\frac{3}{2}\frac{3}{2}$) in Fig. 2] become rapidly resembling that of Fe in ordered magnetic FeAl. It is noteworthy that the spin-up subband is essentially filled, so that any subsequent removal of electrons may take place primarily from the minority-spin subband and thus increase the magnetic moment. Therefore one should expect a clear correlation between fluctuations of charge transfer and those of local magnetic moment over shells of distant Fe neighbors. Apart from the Fe-AS atom, the pronounced enhancement of the magnetic moment, compared to the average value in the ordered alloy, occurs for Fe atoms which are first neighbors to the vacancy at the Al site.

From all four defects considered in the Co–Al system, only the Co-AS develops a magnetic moment which is in agreement with previous observations based on the KKR–Green's function calculations of Stefanou *et al.*[5] Quantitatively, our results differ only slightly from those of Ref. 5: our magnetic moment at the AS Co (1.53 $\mu_{\rm B}$) is almost the same as in pure elemental Co (1.72 $\mu_{\rm B}$ experimentally; 1.55 $\mu_{\rm B}$ as calculated, e.g., in Ref. 6) against 1.22 $\mu_{\rm B}$ in Ref. 5. The total moment at the cluster of nine Co atoms is 2.67 $\mu_{\rm B}$ (2.06 $\mu_{\rm B}$ in Ref. 5). This difference is probably related to the fact that the magnetic moments are attributed to space-filling atomic spheres, which we used in our case, compared to non-overlapping muffin-tin spheres in the KKR–Green's function approach.

An unusual feature in Table I is that in two cases, namely for the Fe vacancies and for the Al AS in FeAl, the Fe atoms which are *most distant* from the defect exhibit quite large magnetic moments. This is most probably an artefact related to a yet too small supercell size. This artefact, which is quite stable against the changes in the calculation setup (more dense k-mesh in the BZ integration etc.), was not reported in earlier LMTO supercell calculations by Gu and Fritsche.[25] They used the same geometry of the 32-atoms supercell (for AS defects) as we did and of course obtained much similar results for the magnetic moments in the vicinity of defects. Our explanation for the artefact is the following: Magnetic moments within different shells of Fe neighbors surrounding the defect exhibit long-range oscillations around the bulk value of 0.76 $\mu_{\rm B}$, as is seen from Table I. For the Fe atoms most distant from the vacancy at Fe and from the Al AS, which are both situated at $2a$ from the defect, the oscillations just tend to be positive. In our particular supercell geometry there is only one of such an Fe atom per supercell, which at the same time is the (fourth

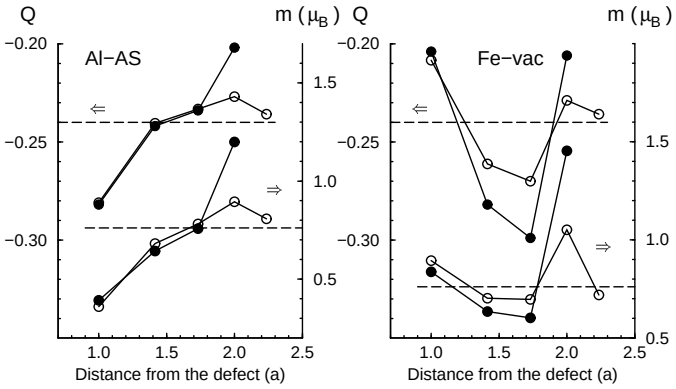

FIG. 4. Charge transfer (left scales) and magnetic moments (right scales) over shells of Fe neighbors to AS Al and Fe vacancy in FeAl. Dots – calculation results for 32-at. supercells; open circles – for 64-at. supercells. Dashed lines indicate the asymptotic values of charge transfer and magnetic moment in ordered FeAl.

nearest) neighbor to six defect sites. The constructive interference of these oscillations coming from six defects is pinned at a single atom, resulting in an anomalously high magnetic moment. In a real defect crystal with no ordering in the mutual orientation of defects there is no physical reason for such a high moment to be pinned at any site far from the defect.

In order to prove that the explanation given above is correct, we have performed the calculations for supercells of increased size (including 64 atoms) for two defect types in question. The magnetic and charge distributions over spheres are shown in Fig. 4 in comparison with the data for the 32-atom supercells, which are listed in Table I. One can see that, while the anomalous magnetic moment at the fourth neighboring Fe site is considerably reduced in a larger supercell, the trends in the vicinity of defects are not as much affected. Therefore the use of 32 atom-supercells for our subsequent analysis is justified. An additional observation seen from Fig. 4 is that charge fluctuations and magnetic fluctuations over spheres behave almost identically. This is due to the manifestation of the above mentioned feature that local charge fluctuations affect essentially the minority-spin subband and hence the net magnetic moment.

For CoAl, the Fermi energy is placed near the minimum between two d-peaks and therefore leads to a loss of magnetic moment in spite of decreasing of charge transfer due to the charge-induced perturbations around the Co-vacancy, Al-vacancy and Al-AS defects. Only the Co-AS defect provides a sufficient decrease in the charge transfer in order to fulfill the Stoner condition and to create the magnetic moment at this site.

It is necessary to point out that planar defects, like the surface, may be expected to affect the magnetism in a similar way as point defects do. In particular, FLAPW 7-layer slab calculations, performed in order to simulate the surfaces of FeAl and CoAl compounds,[44] resulted in

TABLE II. Cohesive properties (eV) at equilibrium lattice constants a (a.u.) of FeAl, CoAl and NiAl

	FeAl		CoAl		NiAl	
	Energy	a	Energy	a	Energy	a
			Formation energy			
Experiment (Ref. 45 and as cited in Ref. 6)	−0.26	5.409	−0.56	5.408	−0.64	5.456
TB-LMTO (Ref. 6)	−0.50	5.364	−0.75	5.317	−0.77	5.377
Present work: Ordered B2	−0.40	5.397	−0.66	5.354	−0.71	5.422
Present work: Disordered	−0.23	5.366	−0.38	5.367	−0.53	5.410
			Magnetic energy			
Ordered B2	−0.02		—		—	
Disordered	−0.05		0.00		—	

a magnetic ordering for FeAl(100) and CoAl(100) surfaces, while NiAl(100) was magnetically dead. The Fe surface atom with a magnetic moment of 2.57 μ_B has up to 0.25 electrons less than the next iron layer atom with a moment of 0.67 μ_B – this is the same trend, but more pronounced, as in our calculation for a Fe atom neighboring the "cavity" of the Al vacancy. In the case of CoAl, the surface atom loses about 0.3 electrons as compared to the atom in the next Co layer, which results in the enhancement of the surface Co moment to 1.12 μ_B.

The changes in the total energies due to the variations of the lattice constants exhibit the expected parabolic behavior. This is shown in Fig. 5, where the results for two different exchange-correlation potentials are presented. Table II includes the results obtained by a parabolic fitting of the total energy data. As pointed out in Sec. II, the data related to ordered compounds, as well as the defect formation energies, have been obtained with non-local corrections to the exchange-correlation, whereas the data for disordered alloys (discussed in more detail below) result from the calculations within the LDA. The calculated equilibrium lattice constants are consistently underestimated by about 1%, with somehow better agreement to the experimental data in the case where the non-local corrections have been included. The comparison with the results of earlier TB-LMTO calculations[6] for ordered TM aluminides, obtained within the same formalism but in the LDA, reveals that the non-local corrections to the LDA produce indeed a systematic improvement of all cohesive properties for the alloys under consideration.

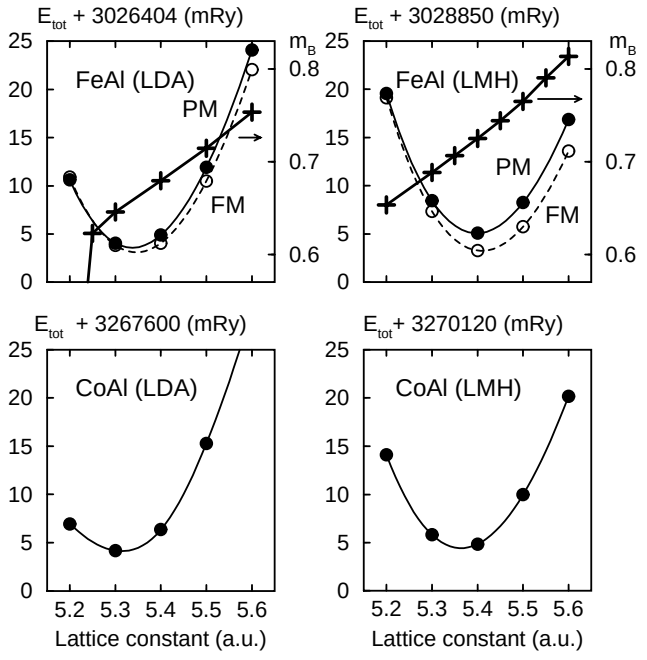

FIG. 5. Total energy (dots, left scale) per formula unit vs. lattice constant in ordered FeAl and CoAl as calculated by TB-LMTO in the LDA and with non-local corrections (LMH).

The cohesive properties have been calculated at equilibrium volumes and are compared with the experimental data available. The experimental data in Table II are from thermochemical formation energy measurements; the total energy of the constituent solids are taken at the equilibrium volume in their respective ground-state structures, i.e. fcc Al and Ni, hcp Co and bcc Fe (ferromagnetic Fe, Co and Ni), calculated with the same setup as used for alloys. The total energies in the TB-LMTO calculation have been also minimized for the defect supercell systems, thus accounting for a uniform lattice dilatation around defects. The corresponding lattice constants are shown in Table III.

It is noteworthy to mention that the calculated heats of formation come out systematically overestimated for all ordered compounds, but to a less extent in the present work than in earlier TB-LMTO calculations[6] with local exchange-correlation. On the other side, they are systematically underestimated by about the same margin in the KKR-CPA calculations (see next Section). Apparently, the properties of real systems fall between the two extremities of complete substitutional disorder and com-

TABLE III. Equilibrium lattice constants a (a.u.) from TB-LMTO supercell calculations

	TM vacancy	Al vacancy	TM antisite	Al antisite
FeAl	5.404	5.401	5.387	5.424
CoAl	5.355	5.337	5.341	5.381

plete ordering with point defects, which are addressed in the present study.

In our calculations ordered CoAl and NiAl fail to develop any magnetic ordered state in agreement with all previous calculations, while FeAl has both ferromagnetic (FM) and nonmagnetic solutions. The earlier LMTO[22] and TB-LMTO[6] studies found the nonmagnetic solution as the ground state within the LDA; our calculation with the LDA puts the magnetic solution minutely lower in energy, actually one cannot reliably claim this (see Fig. 5). With non-local corrections included to the exchange-correlation, the ferromagnetic ground state clearly gains in energy with respect to the nonmagnetic state. The values of the magnetic moment (per cell) for different values of lattice constant are also shown in Fig. 5. As is consistent with other studies on magnetic systems, the non-local exchange-correlation results in somehow larger values of magnetic moments. It should be noted also that ASW fixed-spin-moment calculations[33] provided, in addition, the antiferromagnetic (AFM) state with an energy difference between FM and AFM states of only a tenths of a mRy. Since three possible ground states have very small energy differences, one can conclude that the formation of a spin-glass state seems plausible in the Fe–Al system. The existence of the spin-glass state was indeed detected in Ref. 8.

IV. ELECTRONIC STRUCTURE OF DISORDERED ALLOYS

While the supercell approach aims at studying point defects in otherwise perfect alloys, the limiting case of the ultimate substitutional disorder can be treated by the KKR-CPA approach. Here an atom of each species in the lattice with the probability equal to its concentration can be considered as an impurity in the effective medium, and with complementary probability – as the AS defect. We have performed such calculations for Fe_xAl_{1-x}, Co_xAl_{1-x} and Ni_xAl_{1-x} alloys in the range of compositions $x = 0.4$ to 0.6. From the series of KKR-CPA calculations for different alloy compositions and different volumes per atom we have determined the equilibrium lattice parameters. Their values for $x = 0.5$ are also listed in Table II. In Fig. 6 we show the results of these calculations for Co–Al and Fe–Al systems for both ferromagnetic and nonmagnetic solutions. The magnetic solution is missing in Co_xAl_{1-x} only for $x = 0.4$. For Ni_xAl_{1-x} no magnetic solution has been found in the whole range of concentrations, which have been studied in this contribution.

As it is shown in Fig. 6 the $Co_{0.5}Al_{0.5}$ alloy exhibits the ferromagnetic solution, in contrast to the ordered CoAl compound (see Fig. 5). The total energy difference between ferromagnetic and nonmagnetic ground states is however extremely small, as is listed in Table II. The magnetic moment at the Co site is 0.47 μ_B near the transition point to the nonmagnetic state. The ferromagnetic

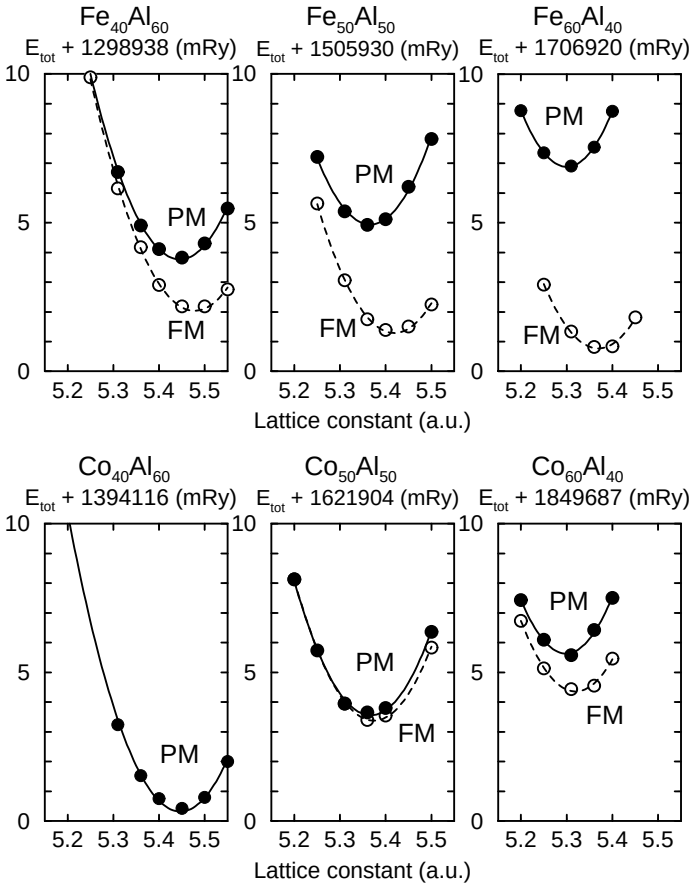

FIG. 6. Total energy (per atom) vs. lattice constant in disordered Fe–Al and Co–Al for several concentrations as calculated by KKR-CPA, for paramagnetic (PM) and ferromagnetic (FM) solutions.

state disappears under pressure but becomes clearly the favorable one for increased volumes in this system.

In order to investigate the type of magnetic instability, we have performed the FSM analysis for the $Co_{0.5}Al_{0.5}$ alloy, with the total energy calculated as a function of fixed magnetic moment and lattice constant. The results of these calculations shown in Fig. 7 indicate the presence of a saddle point between magnetic and nonmagnetic solutions. It means that the phase transition between ferromagnetic and nonmagnetic states occurs as a first-order transition. At the moment, this is only a theoretical prediction, since the fully disordered CoAl alloy was not obtained experimentally and, moreover, the magnetic transition is expected to occur for a somehow expanded lattice. However, this transition can be seen as a kind of pressure-induced transition in the case of Co-rich disordered alloys, as follows from Fig. 6, and it has been really found at low temperatures in the $Co_{0.6}Al_{0.4}$ alloy.[3]

For Fe–Al disordered alloys, the ferromagnetic solutions exist over the whole range of composition $0.4 < x < 0.75$, which has been covered in the present work.

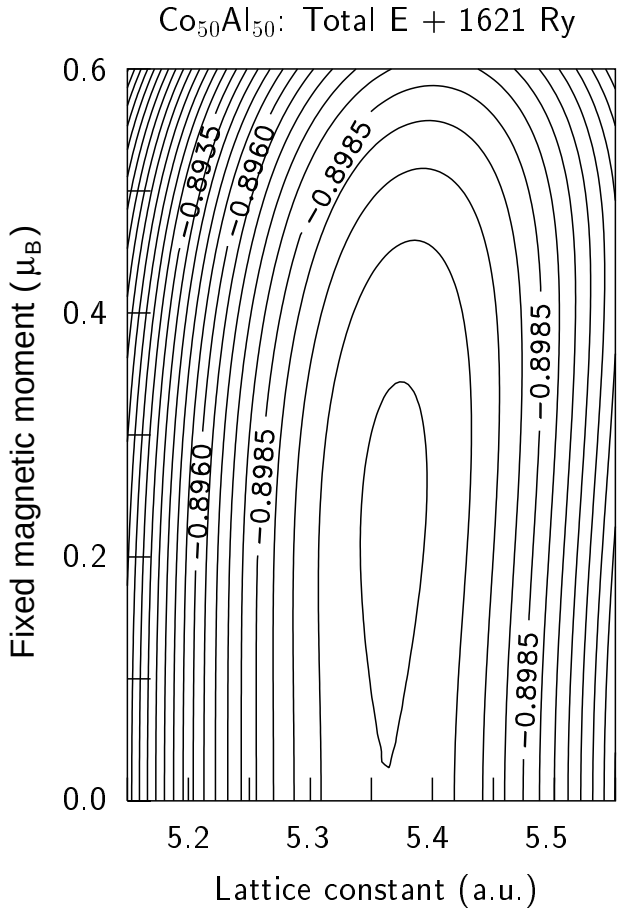

FIG. 7. Total energy vs. lattice constant and magnetic moment calculated by FSM KKR-CPA for disordered $Co_{0.5}Al_{0.5}$.

The results are shown in Fig. 6. The energy difference between ferromagnetic and nonmagnetic solutions increases for Fe-rich disordered alloys, and for the $Fe_{0.5}Al_{0.5}$ alloy we obtain the ferromagnetic ground state already within the LDA approach (see, also, Table IV). Only for the case $x < 0.4$ the nonmagnetic solution can be more stable. It is interesting to point out that for both Co–Al and Fe–Al disordered alloys the minimum of the formation energy coincides with the stoichiometric composition. On the contrary, for the Ni–Al alloy the minimum is shifted to a higher concentration of the transition metal.

The Fe–Al alloys, annealed from high temperatures in order to obtain the perfect disordered state, show the magnetization in a broad range of compositions.[2] We compare these experimental values with the calculated KKR-CPA magnetization per unit cell in Fig. 8, where also the local magnetic moments for Fe and Al atoms are given. Actually, the calculated magnetization decreases slower with the Al concentration than it does in the experimental findings. This can be explained by the change of disordering degree with concentration in the actual samples. The comparison between the experimental and the calculated dependencies of the lattice constant support this possibility (see Fig. 8). The experimental dependence of the lattice constant on composition can be considered as an averaging over local variations of spacing around randomly distributed defects, as affected, e.g., by the heat treatment. The KKR-CPA calculation, on the contrary, gives the equilibrium volume as a smooth monotonic function of the iron concentration. As usual, the magnetization is a function of the equilibrium volume, and an extended lattice provides a larger value of the magnetization. In order to get more insight into the volume trends on disordering, the data on equilibrium lattice constants for defect systems, as estimated from our supercell calculations (see Table III), may be of some use. We did not allow for local (breathing) relaxations of neighbors around the defect because such energy evaluations might be not sufficiently reliable in a calculation done with the ASA. The trends in the uniform lattice expansion, simulating in this case the effect of a lattice dilatation around defects, are usually quite robust and reasonably obtainable in the ASA. The equilibrium lattice constant for a system with an Al-AS defect is 5.424 a.u., whereas that with an Fe-AS defect is 5.387 a.u. The only possibility to understand the experimental trend seen in Fig. 8, i.e. that the lattice constant is relatively independent on the Fe concentration, – is to assume the existence of Al antisite defects even at elevated Fe concentration.

TABLE IV. Disordered alloys formation energies (eV)

Alloy	x	electron/atom	ferro	para
Fe_xAl_{1-x}	0.4	5.00	−0.25	−0.23
	0.5	5.50	−0.28	−0.23
	0.55	5.75	−0.28	
	0.6	6.00	−0.28	−0.20
	0.65	6.25	−0.26	
	0.7	6.50	−0.25	
	0.75	6.75	−0.22	
Co_xAl_{1-x}	0.4	5.40		−0.36
	0.5	6.00	−0.38	−0.38
	0.6	6.60	−0.36	−0.34
Ni_xAl_{1-x}	0.4	5.80		−0.45
	0.5	6.50		−0.53
	0.6	7.20		−0.55

It is very useful to compare the DOS for the disordered alloys series Ni–Al, Co–Al and Fe–Al as we do in Fig. 1 for ordered compounds. This comparison is shown in Fig. 9. As becomes evident from our results, the rigid-band model applies better for any fixed TM-Al composition with different TM components than for the same alloy with different concentrations. In particular, the low-energy structure at about −0.3 eV is present for Ni–Al, Co–Al and Fe–Al alloys with 60% of TM but it disappears for the alloys with smaller TM concentrations. Also, the sharpness of the peak at the Fermi energy remarkably changes with the concentration.

The main features of the DOS profiles for ordered compounds are assigned by Zou and Fu,[7] in the order of in-

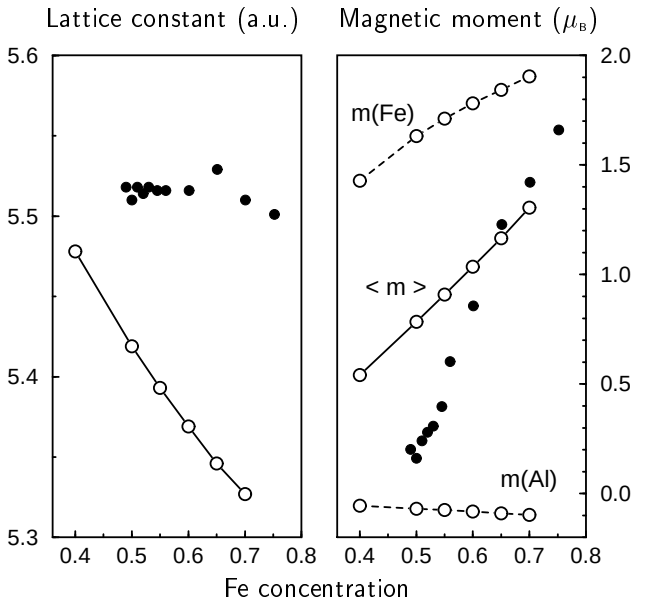

FIG. 8. Theoretical KKR-CPA (open circles) and experimental (dots) concentration dependence of the lattice constant and the magnetic moment in the Fe–Al alloys.

creasing of energy, to the bonding, nonbonding (the peak just below E_F in NiAl) and antibonding states (Fig. 1). A 'pseudogap' separating the bonding and nonbonding states remains well defined in all DOS calculations for ordered compounds. As is shown in Fig. 9, the nonbonding structure completely disappears for disordered alloys. The tendency for the disappearance of the nonbonding peak can be already traced in Figs. 2 and 3 for the AS local DOS, but only the complete disorder leads to the total smearing out of this DOS feature. This effect is favorable for the magnetism, which develops in Co–Al disordered alloys. On the other hand, the disorder reduces the formation energy (see Table II) because the Al to TM charge transfer requires that a late TM atom has as many Al atoms as its nearest neighbors as possible, in order to facilitate the charge transfer and the bonding hybridization.

V. CONCLUSION

We have shown in this paper that the onset of magnetism in the Ni, Co and Fe aluminides is closely related to the defect structure of these compounds. Among the perfectly ordered 1:1 compounds, only FeAl retains a magnetic moment of 0.76 μ_B per atom. In CoAl and NiAl the magnetic moments are totally quenched due to the d-band population. However, in the case of TM-AS defects the value of the magnetic moment for a Fe defect is the same as for a pure bcc iron atom. A large magnetic moment also appears for the Co-AS defect. All nearly disordered Fe–Al alloys exhibit a ferromagnetic ordering

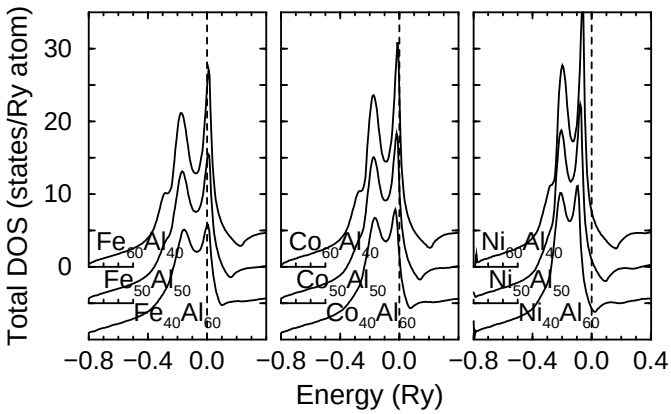

FIG. 9. Total DOS for several concentrations of disordered Fe–Al, Co–Al and Ni–Al alloys as calculated by KKR-CPA.

over the range of compositions 75 at.% to 40 at.% of Fe, i.e. the existence range of the B2 phase. In Co–Al disordered alloys, the onset of ferromagnetism occurs only for a Co concentration larger than 50 at.%. The Ni–Al alloys do not show any magnetic ordering.

The Friedel oscillations around the defects are favorable for the enhancement of magnetic moments in the ferromagnetic FeAl matrix. It means that any defect creates an enhancement of the magnetic moment on neighboring Fe atoms, as charge transfer to these atoms decreases. In the paramagnetic Co–Al matrix, however, these oscillations are only sufficient for creating magnetic moments on Co sites, which are directly neighbors to the Co AS impurities.

ACKNOWLEDGMENTS

This work was supported by the Deutsche Forschungsgemeinschaft. N.I.K. thanks the University of Osnabrück for the kind hospitality during his stay there. Useful comments by J. Kudrnovský are appreciated.

[1] R. J. Wasilewski, J. Phys. Chem. Solids **29**, 39 (1968).
[2] L. G. Booth, H. P. J. Wijn, and G. Zibold, Landolt-Börnstein. Numerical Data and Functional Relationships in Science and Technology. New Series. Group III: Crystal and Solid State Physics, **19**, Magnetic Properties of Metals, subvolume b: Alloys and Compounds of d-Elements with Main Group Elements. Part 1., 363, (1987).
[3] D. J. Sellmeyer, G. R. Caskey, and J. Franz, J. Phys. Chem. Solids **33**, 561 (1972).
[4] A. Amamou and F. Gautier, J. Phys. F: Metal Phys. **4**, 563 (1974).
[5] N. Stefanou, R. Zeller, and P. H. Dederichs, Phys. Rev. B **35**, 2705 (1987).

[6] V. Sundararajan, B. R. Sahu, D. G. Kanhere, P. V. Panat, and G. P. Das, J. Phys.: Condens. Matter **7**, 6019 (1995).
[7] J. Zou and C. L. Fu, Phys. Rev. B **51**, 2115 (1995).
[8] P. Shukla and M. Wortis, Phys. Rev. B **21**, 159 (1980).
[9] A. J. Besnus, A.Herr, and A. J. P. Meyer, J. Phys. F: Metal Phys. **5**, 2138 (1975).
[10] A. N. Bashkatov, L. P. Zelenin, F. A. Sidorenko, and P. V. Gel'd, Phys. Met. Metallogr. **31**, 46 (1971).
[11] M. J. Cooper, Philos. Mag. **8**, 805 (1963).
[12] V. L. Morruzzi, A. R. Williams, and J. F. Janak, Phys. Rev. B **10**, 4856 (1974).
[13] C. Müller, W. Blau and P. Ziesche, Phys. Status Solidi B **116**, 561 (1983); C. Müller, H. Wonn, W. Blau, P. Ziesche, and V. P. Krivitskii, *ibid.* **95**, 215 (1979); C. Müller and P.Ziesche, *ibid.* **114**, 523 (1982).
[14] D. Hackenbracht and J. Kübler, J. Phys. F: Metal Phys. **10**, 427 (1980).
[15] D. Knab and C. Koenig, J. Phys.: Condens. Matter **2**, 465 (1990); C. Koenig and M. A. Khan, Phys. Rev. B **27**, 6129 (1983); J. M. Koch and C. Koenig, Philos. Mag. B **57**, 557 (1988).
[16] Kwang Joo Kim, B. N. Harmon, and D. W. Lynch, Phys. Rev. B **43**, 1948 (1990).
[17] K. Schlemper and L. K. Thomas, Phys. Rev. B **50**, 17802 (1994).
[18] G. A. Botton, G. Y. Guo, W. M. Temmerman, and C. J. Humphreys, Phys. Rev. B **54**, 1682 (1996).
[19] D. Singh, in: *Intermetallic Compounds*, Vol. 1, edited by J. H. Westbrook and R. L. Fleischer (Chichester, John Wiley & Sons, 1994), p. 127.
[20] R. E. Watson and M. Weinert, Phys. Rev. B, **58**, 5981 (1998).
[21] M. J. Mehl, J. E. Osborn, D. A. Papaconstantopoulos, and B. M. Klein, Phys. Rev. B, **41**, 10311 (1990).
[22] B. I. Min, T. Oguchi, H. J. F. Jansen, and A. J. Freeman, J. Magn. Magn. Mater. **54-57**, 1091 (1986).
[23] S. Ögüt and K. M. Rabe, Phys. Rev. B **50**, 2075 (1994).
[24] C. Koenig, N. Stefanou, and J. M. Koch, Phys. Rev. B **33**, 5307 (1986); J. M. Koch, N. Stefanou, and C. Koenig, *ibid.* **33**, 5319 (1986).
[25] Y. M. Gu and L. Fritsche, J. Phys.: Condens. Matter **4**, 1905 (1992).
[26] I. A. Abrikosov, Y. H. Vekilov, A. V. Ruban, and D. Ya. Kats, Solid State Commun. **80**, 177 (1991).
[27] S. K. Bose, V. Drchal, J. Kudrnovský, O. Jepsen, and O. K. Andersen, Phys. Rev. B **55**, 8184 (1997).
[28] W. Lin, Jian-hua Xu, and A. J. Freeman, J. Mater. Res. **7**, 592, (1992).
[29] C. L. Fu, Phys. Rev. B **52**, 3151 (1995).
[30] D. J. Singh, Phys. Rev. B **46**, 14392 (1992).
[31] O. K. Andersen, Phys. Rev. B **12**, 3060 (1975); H. L. Skriver, *The LMTO method* (Heidelberg, Springer, 1984).
[32] O. K. Andersen and O. Jepsen, Phys. Rev. Lett. **53**, 2571 (1984); O. K. Andersen, O. Jepsen, and M. Sob, *Electronic Band Structure and its Applications (Springer Lecture Notes in Physics 283)* (Berlin, Springer, 1997); O. K. Andersen, *Methods of Electronic Structure Calculations* (Singapore, World Scientific, 1994).
[33] V. L. Moruzzi and P. M. Marcus, Phys. Rev. B **47**, 7878 (1993).
[34] W. R. R. Lambrecht and O. K. Andersen, Phys. Rev. B **34**, 2439 (1986); S. Kobayashi and T. Fujiwara, *ibid.* **55**, 7445 (1997).
[35] D. C. Langreth and M. J. Mehl, Phys. Rev. Lett. **47**, 446 (1981); Phys. Rev. B **28**, 1809 (1983).
[36] U. von Barth and L. Hedin, J. Phys. C: Solid State Phys. **5**, 1629 (1972).
[37] P. E. Blöchl, O. Jepsen, and O. K. Andersen, Phys. Rev. B **49**, 16223 (1994).
[38] A. F. Tatarchenko and N. I. Kulikov, Phys. Rev. B **50**, 8266 (1994).
[39] L. Hedin and B. L. Lundqvist, J. Phys. C: Solid State Phys. **4**, 2064 (1971).
[40] D. Vanderblit and S. G. Louie, Phys. Rev. B **30**, 6118 (1984); D. D. Johnson, *ibid.* **38**, 12807 (1988).
[41] A. R. Williams, V. L. Morruzzi, J. Kübler, and K. Schwarz, Bull. Am. Phys. Soc. **29**, 278 (1984).
[42] P. A. Schultz and J. W. Davenport, J. Alloys and Compounds **197**, 229 (1993).
[43] H. Domke and L. K. Thomas, J. Magn. Magn. Mater. **45**, 305 (1984).
[44] A. A. Ostroukhov, V. M. Floka, and V. T. Cherepin, Surface Science **352-354**, 919 (1996).
[45] P. Villars and L. D. Calvert, *Person's Handbook of Crystallographic Data for Intermetallic Phases* **1-3**, (1985).